THE ASTROPHYSICAL JOURNAL, 326:564–573, 1988 March 15

DETAILED STUDY OF THE BARRED SPIRAL GALAXY NGC 4027. II. INTERNAL KINEMATICS

W. D. PENCE,[1,2] K. TAYLOR,[1] K. C. FREEMAN,[3] G. DE VAUCOULEURS,[3,4] AND P. ATHERTON[5,6]

Received 1987 June 15; accepted 1987 September 1

ABSTRACT

The two-dimensional velocity field of the asymmetric barred spiral galaxy NGC 4027 has been mapped with the TAURUS Fabry-Perot interferometer mounted on the Anglo-Australian telescope. The Hα emission line was measured at more than 6000 positions over the galaxy disk to derive maps showing the distributions of central velocity, line width, and line intensity. The intensity map shows that the Hα emission is mainly concentrated in a giant ring 1.7 kpc in diameter which includes the bar and the southern spiral arm. By contrast, the H I emission seems to come mainly from the northern half of the galaxy, suggesting that the H I in the southern half has been depleted by recent star formation. The velocity dispersion of the H II gas is 30 km s^{-1} throughout the galaxy, including the bar, arms, and interarm regions.

A simple axisymmetric kinematic model is able to fit the observed velocity field very well; the RMS velocity residual between the observed and modeled velocities is only 13.9 km s^{-1}, which is not much more than the estimated observation error per point of ± 10 km s^{-1}. The most surprising result is that the center of symmetry of the velocity field coincides to high precision with the center of the bar even though the bar is displaced by 5″ from the center of the outer optical isophotes. This was unexpected because previous lower precision observations, and the theoretical models based on them, suggested that the bar should be significantly displaced from the center of mass of the galaxy.

The derived circular rotation curve has a peak rotational velocity of 160 km s^{-1}, assuming the disk has an inclination of $i = 40°$. The best fitting two-component exponential disk mass model has a total mass of $1.1 \times 10^{10}\ M_\odot$ and a mass to blue luminosity ratio of $M/L_B = 2.7$ at the adopted distance of 10 Mpc. The H I mass fraction is $M_{\rm H\,I}/M = 0.086$ which is typical for late-type spiral galaxies.

There are small systematic departures from circular motion near the bar center and along the minor axis of NGC 4027. An area about 3″ = 150 pc in diameter near the center of the bar has a blueshift of 30 km s^{-1}. The noncircular velocities seen along the minor axis qualitatively agree with the expected streaming motions of the gas around the bar gravitational potential. The apparent effects are rather small in NGC 4027, however, because the long axis of the bar is nearly perpendicular to the line of nodes.

Subject headings: galaxies: individual (NGC 4027) — galaxies: internal motions — galaxies: structure — radio sources: 21 cm radiation

I. INTRODUCTION

The study of the internal dynamics of stars and gas in spiral galaxies continues to be an area of active research in astronomy. This paper contributes to this field by providing new detailed observations of the internal gas motions in the barred spiral galaxy NGC 4027, type SB(s)dm, which is a classic example of a large number of galaxies, including the Magellanic Clouds, which have asymmetric arms and have a bar displaced from the center of the outer isophotes. NGC 4027 was selected for this study because (1) the bar is oriented nearly perpendicular to the line of nodes and thus is ideal for detecting radial motions in the gas along the bar major axis, and (2) previous observations at very low spectral and angular resolution (de Vaucouleurs, de Vaucouleurs, and Freeman 1968, hereafter VVF) have suggested large streaming motions in the gas as it circulates around the bar. With modern instrumentation, it is now possible to obtain much higher quality data than was used in this earlier work.

In a previous paper (Pence and de Vaucouleurs 1986, hereafter Paper I) we derived various photometric parameters of NGC 4027 which will be useful for interpreting the kinematic information to be presented here. Briefly, we derived a distance $\Delta = 10 \pm 1.5$ Mpc which implies an image scale of 48.5 pc $arcsec^{-1}$. The apparent total B magnitude is $B_T = 11.67$ and the corrected total luminosity is $L_T(B) = 4.3 \times 10^9\ L_\odot$ assuming $M_\odot = 5.41$. Four distinct photometric components were found: (1) an elliptical bar, (2) a young H II region population, (3) the spiral arms, and (4) an underlying old disk component, which contribute ~10%, 4%, 36%, and 50% of the total luminosity, respectively.

NGC 4027 is also known as Arp 22 and VV 66; it forms a pair with NGC 4027A of separation 3.′7 and a looser association with the very peculiar pair NGC 4038 and 4039 some 41′ away. These associations may be responsible, at least in part, for the asymmetries in the ionization and velocity fields which are to be discussed here.

II. OBSERVATIONS AND REDUCTION METHOD

NGC 4027 was observed with the TAURUS scanning Fabry-Perot interferometer (Taylor and Atherton 1980;

[1] Anglo-Australian Observatory, Epping, N.S.W.
[2] Space Telescope Science Institute, Baltimore.
[3] Mount Stromlo and Siding Spring Observatories, Australian National University, Canberra (ANU Visiting Fellow 1981–1982).
[4] Department of Astronomy and McDonald Observatory, University of Texas, Austin.
[5] Kapteyn Laboratory, Groningen.
[6] Queensgate Instruments, Sunbury-on-Thames, Middlesex.

Atherton *et al.* 1982) at the Cassegrain focus of the 3.9 m Anglo-Australian Telescope (AAT) on 1982 April 3. The observations of the Hα emission in NGC 4027 were made with an etalon giving a 909 km s^{-1} free-spectral range and with a nearly Gaussian transmission profile of width $\sigma = 0.32$ Å = 15 km s^{-1}. The peak transmission wavelength of the etalon was rapidly stepped by 0.19 Å = 8.7 km s^{-1} increments back and forth across the 17 Å band selected by a prefilter centered on the redshifted Hα line at 6599 Å. The photon counts at each etalon position were numerically integrated into a three-dimensional data cube with 230 × 230 spatial resolution elements (each pixel is 0.″823 square) and 120 spectral channels. The total integration time was 4.7 hr and the average seeing disk was about 3″ FWHM.

The data reduction and analysis was performed on the VAX 11/780 computer at the AAO using the TAURUS data reduction software (TDR) package (Taylor, Hook, and Atherton 1984). Following the initial phase correction and velocity scale calibration of the data cube, an automatic procedure (the AUTOFIT program) was used to examine the spectrum at each spatial position and fit a Gaussian function to any significant emission feature. This produced four two-dimensional maps representing the height, width, and central velocity of the Hα emission line, together with the continuum level, at each position in the galaxy. Various automatic and interactive procedures were then used to clean these maps to remove spurious points (e.g., Gaussian fits with negative heights). In the final analysis, 6174 pixels had a measured emission-line profile. These points are not completely independent, however, since the pixels are about one-third the size of the seeing disk.

The wavelength scale of the emission was calibrated by exposures of a neon source before and after the galaxy observations. In addition, a faint OH night sky line at $\lambda = 6596.53$ Å in the data was used to confirm that the wavelength zero point was correct to within 0.18 Å = 8 km s^{-1}.

The accuracy of each velocity measurement depends on the strength of the emission, but on average the standard error is about 10 km s^{-1} per individual pixel. This was estimated by two methods. First, the deviation of each pixel with respect to the mean velocity of its eight surrounding neighbors has a dispersion of 6 km s^{-1}. This is a lower limit to the actual random error because of the correlation between the velocities of adjacent pixels. As an upper limit to the mean error we note that the RMS scatter between the observed velocity and the circular rotation model to be discussed later is 13.9 km s^{-1}. This overestimates the random errors because this simple model does not account for the noncircular velocities present in NGC 4027.

One particular problem with the data set was caused by internal reflections between the etalon and the interference prefilter which produced ghost images in the northern half of the galaxy of the bright emission regions in the bar and southern arms. Fortunately, because of the north-south velocity gradient in NGC 4027, it was possible to discriminate between the real and ghost images in the northern arm on the basis of their velocity.

III. OBSERVATIONAL RESULTS

a) Hα *Emission Map*

A map of the relative intensity distribution of the Hα emission in NGC 4027 was formed from the product of the Gaussian width and height maps and is shown in Figure 1. The position and relative intensities of 77 discrete emission regions identified in this map are listed in Table 1. Note that the relative intensities are not corrected for possible small variations in the prefilter bandpass across the ~2.′5 diameter field of view.

With this reservation, there is a strong asymmetry in the Hα emission between the north and south halves of NGC 4027; more than 60% of the Hα flux is emitted south of the major axis of the bar. The reality of this asymmetry is confirmed by the broad-band Hα image published by Hodge and Kennicutt (1983) which shows the same effect. Most of the H II regions are concentrated in a giant ring, some 35″ = 1.7 kpc across, which includes the bar, the southeastern spiral arm, and then arcs back around to the bar. No Hα emission could be detected at the center of this ring of H II regions. This ring appearance is quite different from the distribution of continuum emission mapped by the broad-band photographic plates analyzed in Paper I.

It is interesting to compare the total Hα profile, integrated over the whole galaxy, with the H I profile measured by Bottinelli, Gouguenheim, and Paturel (1982*a*, *b*). Figure 2 shows that the H I is stronger on the high-velocity (northern) side while the Hα is concentrated on the opposite side. A natural conclusion from this figure is that the H I in the southern half has been depleted by star formation. If one assumes that the original H I profile was symmetric about the systemic velocity of 1633 km s^{-1} (derived in § IV*b*) as shown by the vertical line in Figure 2, then about one-fourth of the total H I emission is missing on the south side. Since the observed total H I mass is $10^9\ M_\odot$ (for a distance of 10 Mpc), then about $2.5 \times 10^8\ M_\odot$ of H I appears to be missing, presumably condensed into new stars or ionized by the resulting strong UV radiation flux. This effect appears similar to that in some blue compact galaxies which have a chaotic, extended H I distribution with a deficiency of H I gas near the position of the young blue stellar population (Sargent 1986).

The bright H II region near the center of the bar (No. 39 in Table 1) which appears at first glance as the nucleus, is in fact displaced 1.″6 to the east of the center of the bar as defined by the isophotes on the *B*, *V*, and *R* photographic plates discussed in Paper I. The velocity dispersion within this emission region (see Fig. 3) is not significantly higher than in the rest of the galaxy, so it is probably just a normal H II region and not a nuclear emission source. Photometrically there is no evidence of a distinct nuclear component in NGC 4027 on either the broad-band plates or the Hα map. This is not unusual because the nucleus generally becomes less conspicuous in the later stages of the Hubble sequence and essentially vanishes at morphological classes $t > 7$ (de Vaucouleurs 1959; Simien and de Vaucouleurs 1986). The only suggestion for a distinct nucleus in NGC 4027 comes from the blueshifted velocity near the center of the bar (discussed in § Vb) which might indicate the presence of an energetic source at the bar center.

b) *Velocity Dispersion*

The Hα emission-line profile of several typical H II regions is shown in Figure 3. There is no significant difference between the H II velocity dispersion in the bar, arm, or interarm regions of NGC 4027 and the median width of all the measured emission profiles corresponds to a velocity dispersion $\sigma = 30.2$ km s^{-1} (corrected for the instrumental line width of $\sigma_0 = 15$ km s^{-1} measured from the neon calibration lamp). This dispersion is very large compared to that seen in other galaxies and sug-

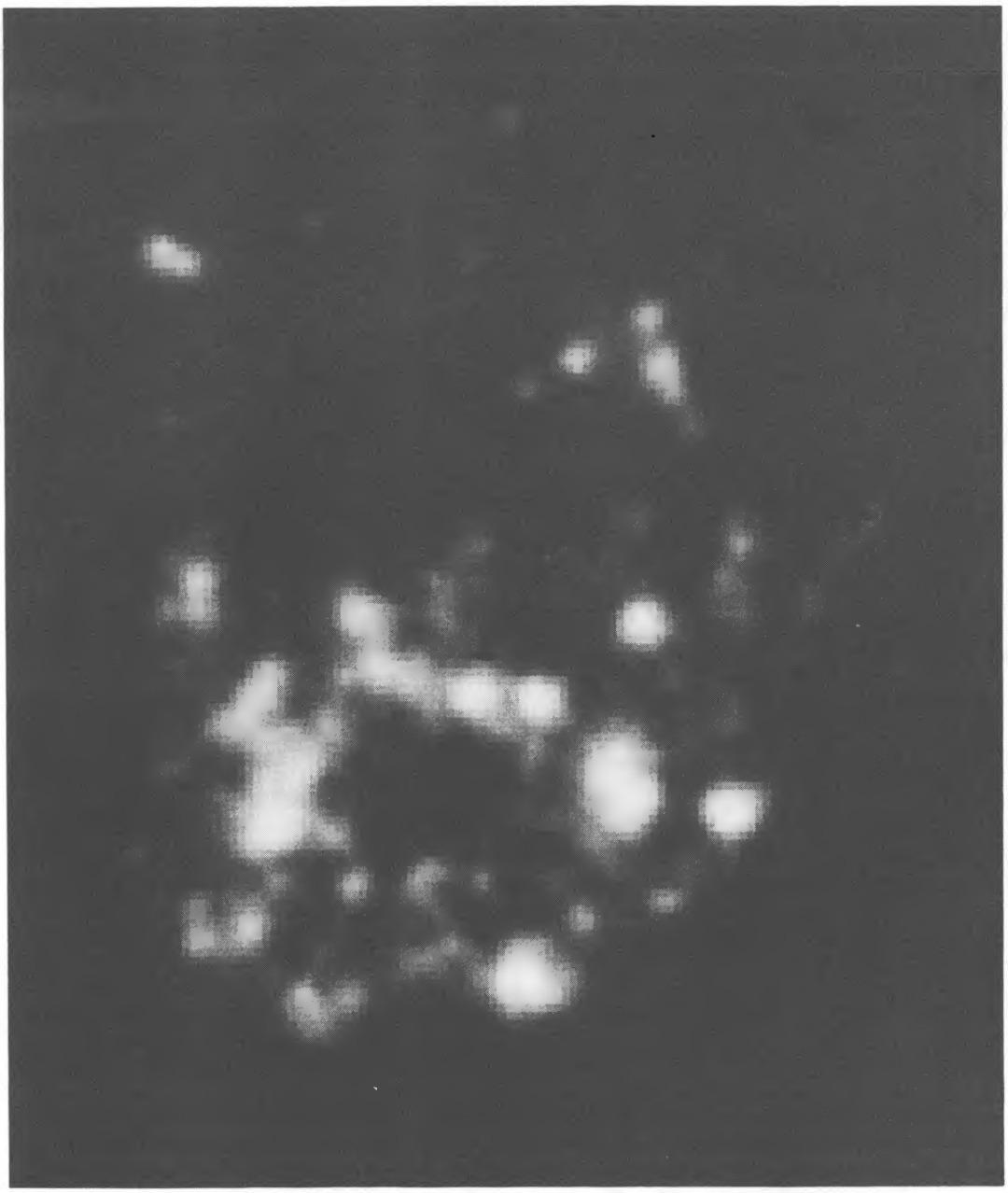

FIG. 1.—Map of the relative intensity of the Hα emission in NGC 4027. Most of the Hα flux is emitted in a giant ring 35″ across which includes the bar and the southern spiral arm. North is at the top, east is to the left, and each image pixel is 0″.823 square.

gests that some unusual heating mechanism is affecting the gas in NGC 4027. Tully (1974), for example, measured $\sigma = 17$–20 km s^{-1} in the H II emission in the disk of M51; only the nuclear lens region of M51 has a velocity dispersion as high as is seen in NGC 4027. The H I z-direction velocity dispersion of spiral galaxy disks is generally even smaller, in the range 8–15 km s^{-1} (Heidmann, Heidmann, and de Vaucouleurs 1971; Warner, Wright, and Baldwin 1973; Emerson 1976).

c) *Velocity Field*

The derived heliocentric velocity field of NGC 4027 is shown in Figure 4 superposed on a broad-band red image of the galaxy. The general "spider diagram" shape of the iso-velocity contours shows that the gas motion is dominated by rotation. Assuming that the main arms are trailing, the east side of the galaxy is nearest to us which is consistent with the fact that the dust lanes appear stronger on the east side where they are seen in projection against the background galaxy luminosity (de Vaucouleurs 1958). Figure 5 shows the observed radial velocity (*solid line*) along the major axes compared with the rotation curve derived in § IV (*dashes*) and with the velocity profile derived by VVF (*dots*). Our new higher quality observations do not confirm the large apparent rise and then dip in velocity on the north side which was a major item of discussion in VVF and which was the key feature in their models. Because of this difference most of our conclusions differ substantially from those in VVF.

TABLE 1

H II REGIONS IN NGC 4027

No.	X	Y	I	No.	X	Y	I
1	−37	−37	7	40	−2	12	12
2	−36	−16	11	41	−2	16	14
3	−33	45	37	42	−1	−18	18
4	−33	9	17	43	0	−28	29
5	−32	28	10	44	2	58	12
6	−32	−7	13	45	2	−28	121
7	−31	44	32	46	4	−5	21
8	−30	12	38	47	4	31	15
9	−30	9	30	48	5	0	72
10	−30	−21	19	49	6	−29	39
11	−30	−25	25	50	7	−12	14
12	−26	−2	34	51	7	−19	12
13	−25	−23	37	52	9	−22	25
14	−23	1	41	53	9	34	43
15	−23	−4	39	54	11	−15	21
16	−22	−13	73	55	12	−7	74
17	−22	−18	20	56	14	−10	88
18	−22	10	8	57	15	18	12
19	−20	−7	54	58	15	7	83
20	−19	−30	29	59	16	38	33
21	−18	48	10	60	17	33	41
22	−17	−33	19	61	18	−21	22
23	−17	−26	13	62	19	2	11
24	−16	−14	26	63	21	27	14
25	−16	−3	27	64	23	43	9
26	−15	−30	22	65	24	−12	103
27	−15	2	28	66	24	12	19
28	−14	−19	28	67	25	−2	13
29	−14	8	48	68	26	16	25
30	−12	2	40	69	26	8	15
31	−8	2	36	70	30	61	8
32	−7	−26	19	71	31	4	8
33	−7	−18	25	72	31	48	8
34	−6	−21	15	73	33	9	11
35	−6	12	18	74	35	13	9
36	−5	8	19	75	37	47	8
37	−4	−26	19	76	39	17	12
38	−2	44	7	77	40	28	7
39	−2	0	76				

NOTE.—X and Y in arseconds positive W and N of bar center.
I = intensity in arbitrary units.

IV. AXISYMMETRIC MODEL

a) *Model Description*

As a first step toward understanding the dynamics of NGC 4027 we fitted a simple circular rotation model to the observed velocity field using the method described by Davoust and de Vaucouleurs (1980). This model will form a frame of reference for analyzing the noncircular motions. The axisymmetric rotation model requires four basic parameters (systemic velocity, inclination, position angle of line of nodes, and the coordinates of the center of rotation) as well as a rotation curve (i.e., the circular velocity as a function of radius). Using an iterative procedure, trial values for the basic parameters are adopted, and then the observed velocities are deprojected to find the average rotation velocity within concentric annuli of increasing radii (individual points are weighted by the cosine of the angle with the line of nodes). Then by inverting the procedure this mean rotation curve is used to calculate the expected radial velocity at the position of each of the velocity measurements. The standard deviation of the difference between the observed and calculated velocities is used to judge the goodness of fit of the model. Different values for the four input parameters are then tried until the combination which produces the smallest standard deviation is found. The observed velocity measurements cover both arms and the central bar region fairly completely, so no attempt was made to try to weight the points to allow for possible nonuniform sampling of the velocity field.

In practice this method cannot be used to derive the inclination because of the strong mathematical coupling with the amplitude of the rotation curve; as the inclination is made smaller, the derived rotational velocities increase, but the RMS fit of the model hardly changes. Therefore we adopted $i = 40° \pm 2°$ derived in Paper I from the axial ratio of the outer isophotes.

b) *Derived Axisymmetric Kinematic Parameters*

A search of the remaining parameter space found that the smallest standard deviation of $\sigma = 13.9$ km s^{-1} was given by the following values:

center of rotation X_0, Y_0 = center of bar ($\pm 1''$);
position angle of line of nodes $\theta = 164° \pm 2°$;
systemic velocity $V_s = 1633 \pm 2$ km s^{-1} (internal error).

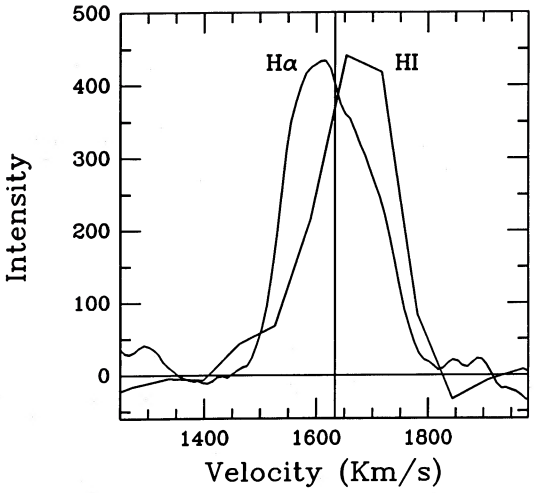

FIG. 2.—Comparison of the total integrated H I and H II flux profiles in NGC 4027. There is a deficiency of H I emission on the low-velocity (southern) side of the galaxy, which is where the H II emission is strongest. This suggests that the recent star formation has depleted the H I gas in the southern half of the galaxy.

That the dynamic center should coincide so well with the center of the bar (as defined by the photographic isophotes) was quite unexpected. Nearly all previous work on the Magellanic-type barred spiral galaxies (see review by de Vaucouleurs and Freeman 1972) and, in particular, the previous study of NGC 4027 by VVF, concluded that the bar is displaced from the center of mass. Also, most theoretical work on the dynamics of these systems have assumed this as a starting hypothesis (de Vaucouleurs and Freeman 1972; Christiansen and Jefferys 1976). In VVF it was concluded that the bar is displaced 4″.8 to the south of the center of mass, based on a cubic polynomial fitted to the rotation curve. However, as is shown in Figure 5, our new data do not confirm the large rotational velocities on the northern side of the galaxy which VVF interpreted as due to streaming motions around the displaced bar.

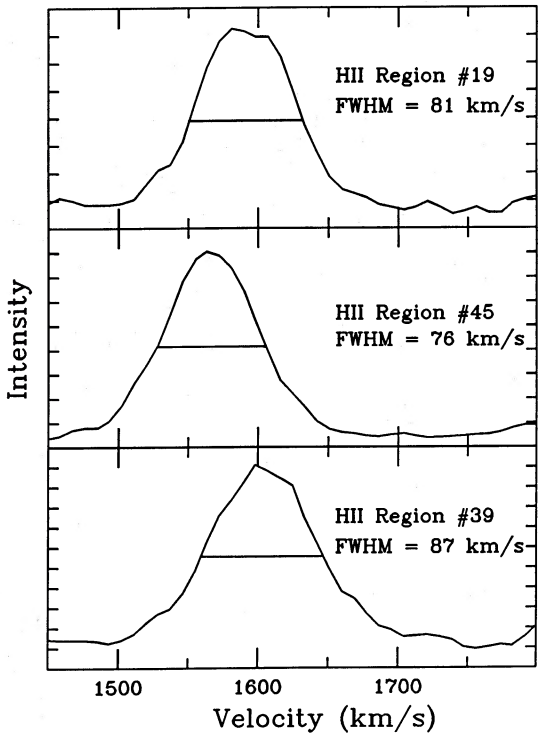

FIG. 3.—The Hα emission line profile observed in several typical H II regions in NGC 4027. The H II region number corresponds to the number given in Table 1. The measured widths of the profiles have not been corrected for the instrumental broadening of $\sigma = 15$ km s^{-1}.

The position angle of the kinematic major axis agrees well with the photometric major axis (P.A. = 167° ± 6°) derived in Paper I. In view of the displacement between the center of the outer isophotes and the center of mass it is in fact surprising that the agreement is so good. We will adopt 165° ± 2° as the P.A. of the line of nodes.

The derived systemic velocity, $V_s = 1633$ km s^{-1}, is only in fair agreement with most of the previous observations. The discrepancy with the 21 cm velocity, $V_{21} = 1677$ (Bottinelli, Gouguenheim, and Paturel 1982*a*, *b*) has already been discussed above and suggests that the recent star formation in the southern (low-velocity) half of the galaxy has depleted the H I emission from that side. This effect is of general importance, since it means that the measured 21 cm velocity is not always a good measure of the center-of-mass velocity of a galaxy. Neglecting some early approximate optical velocity measurements, $V = 2000$ (Struve 1940) and $V = 1844 \pm 88$ (Mayall and de Vaucouleurs 1962), the TAURUS velocity is in fair agreement, within the combined errors, with $V = 1671 \pm 10$ (VVF; de Vaucouleurs and de Vaucouleurs 1967) and $V = 1637 \pm 30$ (de Vaucouleurs 1967). As mentioned before, the measured wavelength of a night sky OH line in the TAURUS data differs by only 8 km s^{-1} from the laboratory value.

The best-fitting rotation curve, given by the mean deprojected velocity of all the points (weighted by the cosine of the angle with the line of nodes) with successive 3″ wide annuli, is shown in Figure 6. It is characterized by a rapid rise out to a radius of 10″ = 0.5 kpc where the curve levels off at $V_c = 120$ km s^{-1}. The maximum rotational velocity of 160 km s^{-1} is reached at a radius of about 53″ = 2.5 kpc.

The outer part of the rotation curve decreases faster than is possible for any real mass distribution, which implies that the assumption of purely circular motion throughout the galaxy is incorrect. Because of this, the mass of the galaxy as derived from this "rotation" curve is ambiguous; the Keplerian mass within the maximum velocity measurement of $V_c = 160$ km^{-1} at $r = 2.5$ kpc is $1.49 \times 10^{10}\ M_\odot$, whereas the mass within the outer velocity measurement of $V_c = 110$ km s^{-1} at $r = 3.4$ kpc is only $9.6 \times 10^9\ M_\odot$. In the following section we use a two-component mass model to derive a better estimate of the total mass.

c) Two-Component Mass Model

The equivalent luminosity profile of NGC 4027 (Fig. 9, Paper I) can be well fitted as the sum of two exponential distributions, one representing the disk and one representing the bar. On the assumption that the mass is distributed in a similar manner (i.e., the mass-to-light ratio is a constant, independent of radius in each component), then one can use the observed effective radius and surface brightness of the two components, along with the tables of normalized rotation curves published by Monnet and Simien (1977), to derive the expected rotation curve for any assumed M/L values. Using the photometric parameters given in Paper I, the luminosity distribution of the

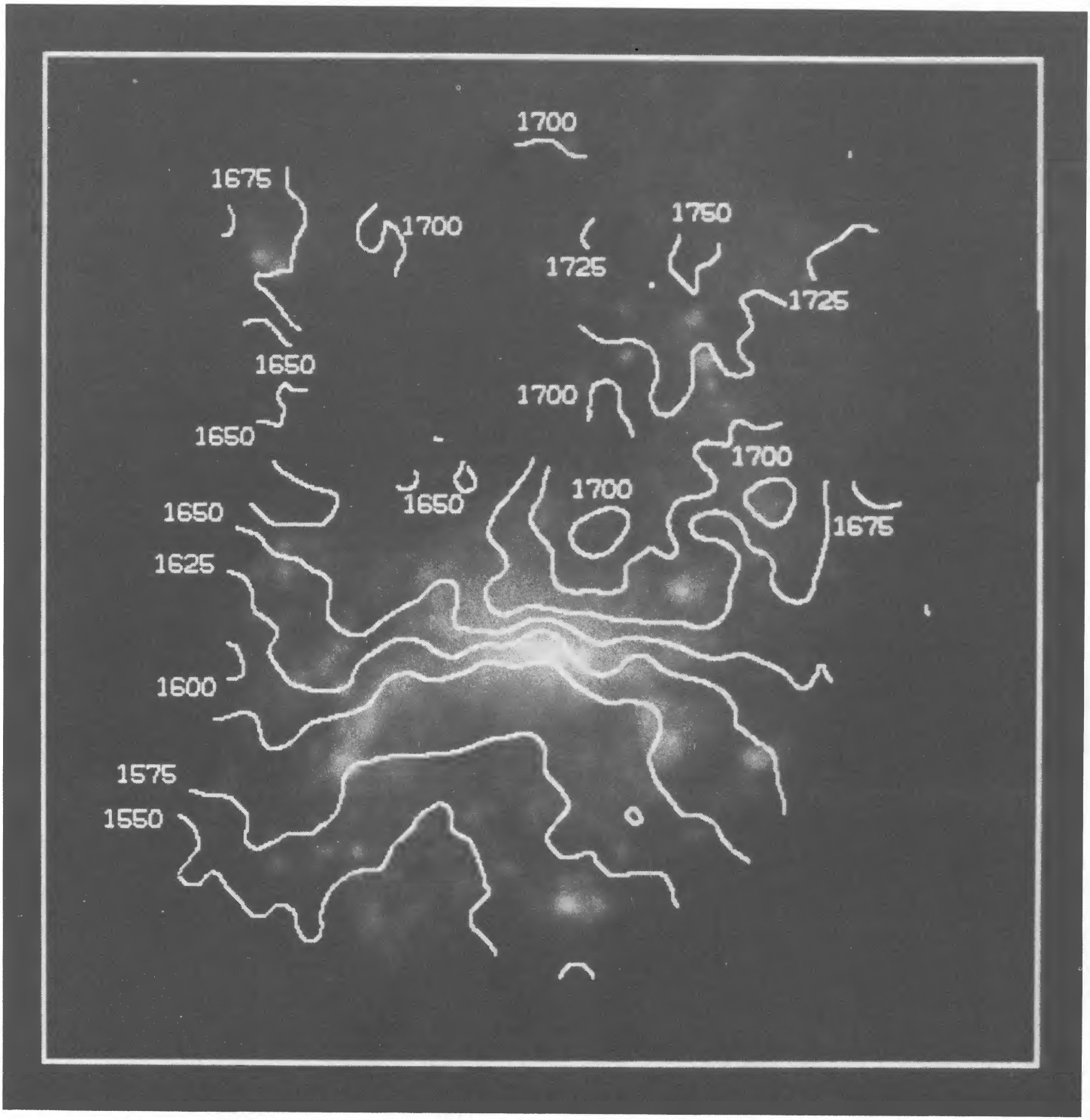

FIG. 4.—The derived isovelocity contour map superposed on an *R* band image of NGC 4027. North is at the top and the frame is 2′ square. The roughly symmetric " butterfly " shaped contour pattern shows that the gas is predominately flowing in circular rotation. Small effects due to noncircular motions are indicated by the wiggley lines in the contour lines near the center of the bar, and by the fact that the contours close to the systemic velocity of 1633 km s^{-1} are not perpendicular to the line of nodes.

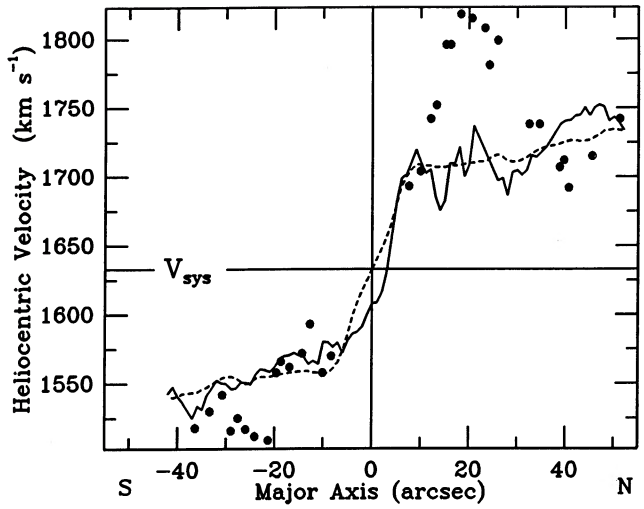

FIG. 5.—The observed velocities along the major axis of NGC 4027 (*solid line*). The best-fitting circular rotation curve for the model described in the text is shown by the dotted line. For comparison, the major axis velocity profile derived by VVF (normalized to a systemic velocity of 1633 km s^{-1}) is shown by the filled circles. Our new data do not confirm the large peak in velocity on the northern side of the galaxy which VVF had interpreted as being due to streaming motions around the bar.

disk is given by $\mu_B(a) = 20.0 + 3.22a$ where the a is the distance along the major axis expressed in arcminutes. The effective radius of the disk is then $a_e = 1644$ pc, and the surface brightness at this radius is $I_e = 150\ L_\odot\ \mathrm{pc}^{-2}$ (corrected for galactic extinction, $A_B = 0.27$ mag). Similarly, the equivalent luminosity profile of the bar is given by $\mu_B(a) = 18.18 + 0.405r^*$ where $r^* = (ab)^{1/2}$ is the equivalent radius of the elliptical bar expressed in arcseconds. (The equivalent bar profile is used instead of the major axis profile to approximate an axisymmetric bar mass distribution.) The effective radius of the bar component is then derived to be 218 pc, and the effective surface brightness is $I_e = 810\ L_\odot\ \mathrm{pc}^{-2}$.

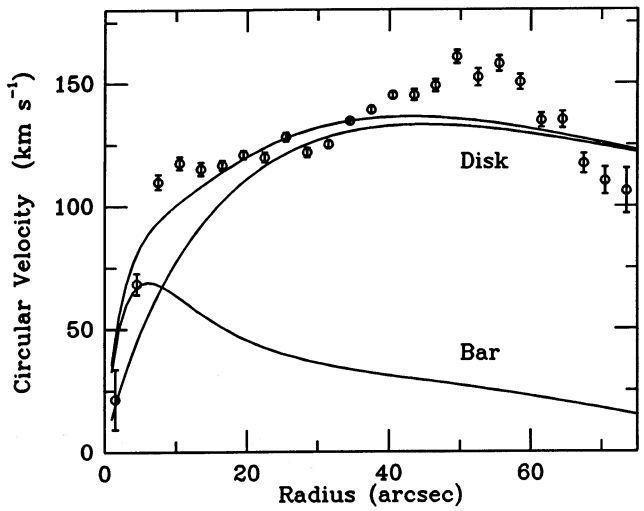

FIG. 6.—The rotation curve of NGC 4027 derived from the best-fitting axisymmetric kinematic model (*circles*) is compared with the rotation curve produced by a two exponential component model (*upper solid line*). The rotation curves for the disk and bar components are also shown separately.

The circular rotational velocity as a function of radius, $V(r)$ of each exponential disk component is given by $V^2(r) = 0.0172 f I_e r_e q_a C(r)$ where $f = M/L$ in solar units, $q_a = 0.77$ is the apparent axial ratio of the galaxy, and $C(r)$ is tabulated by Monnet and Simien (1977) for ellipsoids of various intrinsic axis ratios. For NGC 4027 we assumed axis ratios of 0.1 and 0.2 for the disk and bar, respectively, but the resulting rotation curve depends only slightly on this assumption. The total rotation curve produced by this two-component model was then calculated for various assumed values of M/L for comparison with the observed rotation curve. The basic conclusion from all these calculations is that none of these models can reproduce the observed rotation curve very satisfactorily. As shown in Figure 6 for one of the best-fitting cases, M/L(disk) = 3 and M/L(bar) = 1.2, the bar mass model is too centrally concentrated to reproduce the rotation curve for $r < 10''$, and no physical mass distribution can match the rapid decline in velocity for $50'' < r < 75''$. We attribute most of the discrepancy between this model and the observations to noncircular motions as discussed in the following section.

Even though this model does not fit the rotation curve in detail, it can be used to give a fairly representative value of the total mass. For the case shown in Figure 6, the total mass is 1.14×10^{10} with the bar contributing only 4% of the total. Using the total blue luminosity from Paper I, this gives a mass-to-luminosity ratio of $M/L_B = 2.7$ and a H I mass fraction of $M_{\mathrm{H\,I}}/M = 0.086$, which are both typical for late-type spiral galaxies.

V. NONCIRCULAR MOTIONS

Modeling the nonaxisymmetric velocity field of a galaxy is in general quite complicated, and it is beyond the scope of this paper to attempt to construct a detailed dynamical model to fit the observed velocity field of NGC 4027. Instead we have taken the approach of subtracting the best-fitting circular model from the observed field, and then qualitatively interpreting the resulting residual map. This method will, by definition, minimize the velocity residual map and in the presence of large noncircular motions will even bias the best-fitting circular model. In this particular case, however, the noncircular motions seem to be quite small, so the circular model is probably not significantly affected. The fact that the derived center of rotation agrees exactly with the photometric center of the bar suggests that the circular model is not severely biased.

a) Observed Residuals

The noncircular motions in NGC 4027, calculated by subtracting the radial velocity component of the derived circular rotation curve (§ IV*b*) from each observed velocity measurement, is shown in Figure 7. While the map appears rather chaotic, there is some symmetry present in that the largest velocity residuals tend to be correlated with the direction of the bar: the near side (east) of the bar shows positive residuals of $+10$ to $+20$ km s^{-1} while the far side shows negative residuals of -10 to -20 km s^{-1}. The central bar region also shows relatively large negative residuals. These deviations can be better seen in Figure 8 which shows the radial velocity measured along the minor axis. Most of the other areas of residual velocity seen in Figure 7 are smaller in amplitude and show no obvious correlation with any morphological features of the galaxy. The following sections examine the noncircular motions in the central region in more detail.

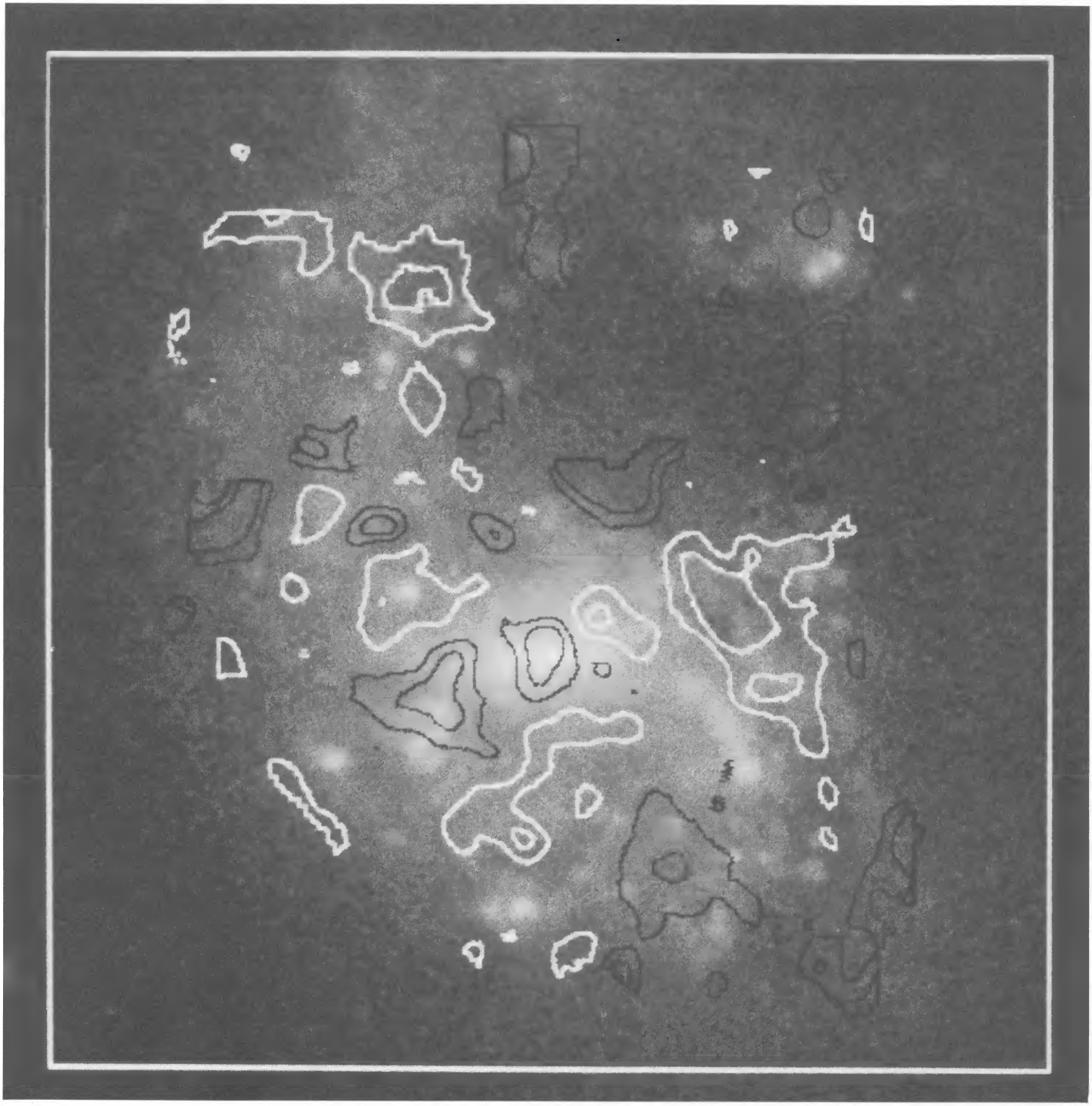

FIG. 7.—The line-of-sight residual velocity contour map derived by subtracting the radial velocity predicted by the best-fitting axisymmetric model from the observed velocity field. Positive residual velocities of +10 and +20 km s^{-1} are shown by the white contours, and negative residuals of −10 and −20 km s^{-1} are shown in black. The largest residuals lie along the minor axis and are consistent with the expected noncircular motions due to streaming motions around the bar. The scale and orientation are the same as in Fig. 4.

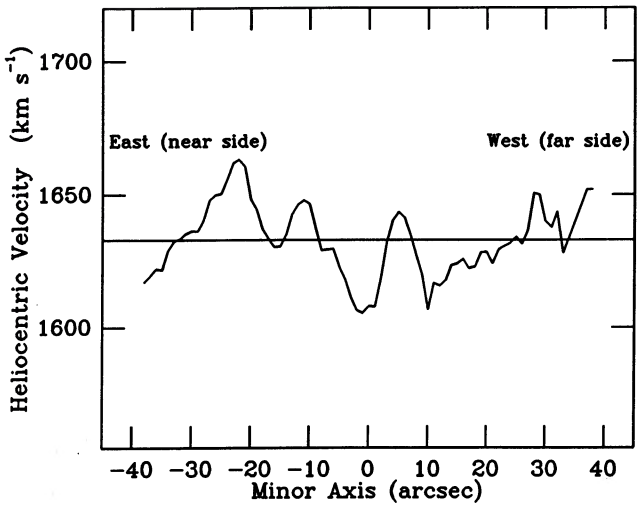

FIG. 8.—Plot of the residual noncircular motions along the minor axis of NGC 4027. The residuals are mainly positive on the near side of the galaxy and negative on the opposite side. There is an outflow of gas (-30 km s^{-1}) close to the center of the bar.

b) Central Blueshift

The Hα emission near the center of the bar shows a blueshift relative to the systemic velocity of the galaxy. Examination of the individual Hα line profiles at the highest possible spatial resolution shows that the blueshift has a maximum amplitude of -30 km s^{-1} and extends over a 3″ diameter area (comparable to the seeing disk) centered 1″ north and 1″ east of the photometric center of the bar. This is about half way between the bar center and the bright central H II region (No. 39 in Table 1). The Hα emission here has a velocity dispersion of only 30 km s^{-1} which is the same as most other H II regions throughout NGC 4027, so this does not appear to be associated with a true galaxy nucleus. This supports the conclusion from Paper I that there is no evidence in the photometry for a distinct nuclear component. The most plausible explanation for the anomalous central blueshift is that it arises from an H II region at a projected distance of 1″ = 50 pc from the center of the bar which has a peculiar motion of 30 km s^{-1} with respect to the surrounding material.

Alternatively, one might explain this blueshift in terms of the expected gas streaming motions around the bar. The main difficulty with this explanation is that all the models of barred spiral dynamics predict velocity fields which have mirror symmetry about the nucleus. Thus one would expect to see a redshifted area on the opposite side of the nucleus, which is not observed. Dust might be obscuring the redshifted area, but there is no evidence in the photometry presented in Paper I for any substantial amounts of reddening in this region.

A more speculative explanation for the central blueshift is that it might be related to the systematic shifts of the nuclear emission lines seen in many active galaxies. Heckman *et al.* (1981) and Wilson and Heckman (1985) discuss surveys of active nuclei which show evidence of systematic velocity shifts, predominantly toward the blue, which can be modeled by radial mass motions near the nucleus. It would seem unlikely though that this mechanism could account for the central blueshift in a galaxy like NGC 4027 which has no visible nucleus.

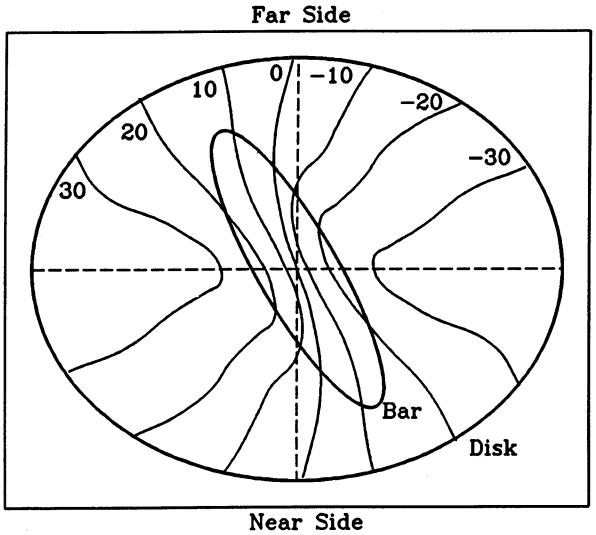

FIG. 9.—Schematic diagram of the expected isovelocity contours for a barred galaxy observed in the same orientation as NGC 4027. The streaming motions of the gas around the bar skew the isovelocity contours to lie nearly parallel to the long axis of the bar and produce positive residual velocities along the near side of the minor axis and negative velocities on the far side. This effect is observed in NGC 4027, but has a small amplitude because the bar is only 8° from being perpendicular to the line of nodes.

c) Oval Streaming around the Bar

There have been numerous detailed studies of the expected gas streaming motions around a bar (van Albada and Roberts 1981; Schwarz 1981; van Albada and Sanders 1982; and references therein) which should be relevant to NGC 4027. While it would be of great interest to make a detailed comparison between these theories and the observed velocity field, it is beyond the scope of the present paper to reproduce the complex hydrodynamical calculations involved in the theories. We can qualitatively show, however, that NGC 4027 exhibits the predicted streaming motions.

The first-order effect of the oval gas motion around a bar is to make the isovelocity contours lie more parallel to the main axis of the bar, causing the kinematic major and minor axes of the galaxy (defined as the position angles with maximum and minimum radial velocity gradients) to become skewed. This effect is apparent in NGC 4027 where the major axis is at a position angle of 165° ± 2°, as derived from both the photometry and from the kinematics, and the kinematic minor axis, as defined by the isovelocity contours near the systemic velocity of 1633 km s^{-1}, lies at P.A. ≈ 81°, i.e., skewed 6° toward the bar axis at P.A. = 83°. As shown in Figure 9, this skewness produces positive residual velocities on the near side of the minor axis, and negative residuals on the far side, just as is seen in NGC 4027.

It is perhaps surprising that the observed noncircular velocity residuals are so small in NGC 4027. Intuitively, one would have expected to find much larger amplitude noncircular motions in a galaxy which has such an obviously asymmetric visual appearance: the northern spiral arm is much more extended than the southern ones, the bar is displaced from the center of symmetry of the outer disk, and both the Hα and H I distributions are asymmetric. Why then should the velocity field appear to be so normal and relatively undistorted?

To a large extent, this paradox is due to the fact that the bar in NGC 4027 is viewed nearly end on. As illustrated by van Albada and Roberts (1981), among others, the velocity field of

galaxies in which the bar is either perpendicular or parallel to the line of sight should appear symmetric, similar to a galaxy with pure circular rotation, except possibly for subtle effects caused by the shock fronts along the leading edges of the more massive bars. It is only when the bar is oriented at about 45° to the line of sight that pronounced distortions are seen in the isovelocity contours. Pence and Blackman (1984) confirmed this effect by classifying the velocity fields of all the well-studied barred spiral galaxies available in the literature. It was found that the three galaxies whose bars are oriented close to 45° to the line of sight all show large distortions in their velocity fields as predicted, but that all eight of the remaining galaxies, whose bars are either oriented nearly parallel or perpendicular to the line of sight, show no large velocity distortions and can generally be well fitted by simple circular rotation models. Thus NGC 4027 is completely consistent with the observations of other barred spiral galaxies.

One major difference between NGC 4027 and the other well-studied barred galaxies is that the bar is significantly displaced from the center of symmetry of the outer disk isophotes. Previously, it had been assumed that the old disk is the best tracer of the mass distribution of a galaxy, and thus the bar must be displaced from the center of mass and rotation in the galaxy. The results of the present analysis, however, show that the bar still marks the center of mass and rotation in NGC 4027.

The TAURUS interferometer was built by P. Atherton and K. Taylor, the observations with the AAT were made by K. Taylor (with K. C. Freeman and G. de Vaucouleurs watching) and the reduction and analysis was mainly by W. D. Pence using software originally developed by R. N. Hook and K. Taylor, G. de Vaucouleurs thanks the Australian National University for a visiting fellowship during 1981–1982.

REFERENCES

Atherton, P. D., Taylor, K., Pike, C. D., Harmer, C. F., Parker, N., and Hook, R. N. 1982, *M.N.R.A.S.*, **201**, 661.
Bottinelli, L., Gouguenheim, L., and Paturel, G. 1982*a*, *Astr. Ap. Suppl.*, **47**, 171.
———. 1982*b*, *Astr. Ap. Suppl.*, **50**, 101.
Christiansen, J. H., and Jefferys, W. H. 1976, *Ap. J.*, **205**, 52.
Davoust, E., and de Vaucouleurs, G. 1980, *Ap. J.*, **242**, 30.
de Vaucouleurs, G. 1958, *Ap. J.*, **127**, 487.
———. 1959, *Handbuch der Physik*, Vol. 53, ed. S. Flugge (Berlin: Springer-Verlag), p. 275.
———. 1967, in *IAU Symposium 30*, p. 91.
de Vaucouleurs, G., and de Vaucouleurs, A. 1967, *A.J.*, **72**, 730.
de Vaucouleurs, G., de Vaucouleurs, A., and Freeman, K. C. 1968, *M.N.R.A.S.*, **139**, 425 (VVF).
de Vaucouleurs, G., and Freeman, K. C. 1972, *Vistas Astr.*, **14**, ed. A. Beer (Oxford: Pergamon), p. 163.
Emerson, D. T. 1976, *M.N.R.A.S.*, **176**, 321.
Heckman, T. M., Miley, G. K., van Breugel, W. J. M., and Butcher, H. R. 1981, *Ap. J.*, **247**, 403.
Heidmann, J., Heidmann, N., and de Vaucouleurs, G. 1971, *Mem. R.A.S.*, **75**, 85.
Hodge, P. W., and Kennicutt, R. C. 1983, *A.J.*, **88**, 296.
Mayall, N. U., and de Vaucouleurs, A. 1962, *A.J.*, **67**, 363.
Monnet, G., and Simien, F. 1977, *Astr. Ap.*, **56**, 173.
Pence, W., and Blackman, C. P. 1984, *M.N.R.A.S.*, **210**, 547.
Pence, W., and de Vaucouleurs, G. 1986, *Ap. J.*, **298**, 560 (Paper I).
Sargent, W. 1986, talk presented at the STScI Stellar Populations Conference, Baltimore.
Schwarz, M. P. 1981, *Ap. J.*, **247**, 77.
Simien, F., and de Vaucouleurs, G. 1986, *Ap. J.*, **302**, 565.
Struve, O. 1940, *Pub. A.S.P.*, **52**, 140.
Taylor, K., and Atherton, P. D., 1980, *M.N.R.A.S.*, **191**, 675.
Taylor, K., Hook, R. N., and Atherton, P. D. 1984, in *Proc Conference on Indirect Imagining*, ed. J. A. Roberts (Sydney), 379.
Tully, R. B. 1974, *Ap. J. Suppl.*, **25**, 415.
van Albada, G. D., and Roberts, W. W., Jr. 1981, *Ap. J.*, **246**, 740.
van Albada, T. S., and Sanders, R. H. 1982, *M.N.R.A.S.*, **201**, 303.
Warner, P. J., Wright, M. C. H., and Baldwin, J. E. 1973, *M.N.R.A.S.*, **163**, 163.
Wilson, A. S., and Heckman, T. M. 1985, in *Astrophysics of Active Galaxies and Quasi-Stellar Objects*, ed. J. Miller (Mill Valley: University Science Books), p. 39.

PAUL D. ATHERTON: Queensgate Instruments, 112 Windmill Rd., Sunbury-on-Thames, Middlesex, U.K.

GERARD DE VAUCOULEURS: Department of Astronomy, The University of Texas, Austin, TX 78712

KENNETH C. FREEMAN: Mt. Stomlo Observatory, Private Bag, Woden P.O., Canberra, ACT. 2606, Australia

WILLIAM D. PENCE: Space Telescope Science Institute, Homewood Campus, Baltimore, MD 21218

KEITH TAYLOR: Anglo-Australian Observatory, P.O. Box 296, Epping, N.S.W. 2121, Australia